



Evolving Simple Models of Diverse Intrinsic Dynamics in Hippocampal Neuron Types

Siva Venkadesh¹, Alexander O. Komendantov¹, Stanislav Listopad², Eric O. Scott³, Kenneth De Jong³, Jeffrey L. Krichmar² and Giorgio A. Ascoli^{1*}

¹ Center for Neural Informatics, Structures, and Plasticity, Krasnow Institute for Advanced Study, George Mason University, Fairfax, VA, United States, ² Cognitive Anteater Robotics Laboratory, Department of Cognitive Sciences, University of California, Irvine, Irvine, CA, United States, ³ Adaptive Systems Laboratory, Krasnow Institute for Advanced Study, George Mason University, Fairfax, VA, United States

OPEN ACCESS

Edited by:

Sharon Crook,
Arizona State University, United States

Reviewed by:

Jesus Garrido,
University of Granada, Spain
Thierry Ralph Nieuw,
Luigi Sacco Hospital, Italy

*Correspondence:

Giorgio A. Ascoli
ascoli@gmu.edu

Received: 21 November 2017

Accepted: 21 February 2018

Published: 13 March 2018

Citation:

Venkadesh S, Komendantov AO, Listopad S, Scott EO, De Jong K, Krichmar JL and Ascoli GA (2018) Evolving Simple Models of Diverse Intrinsic Dynamics in Hippocampal Neuron Types. *Front. Neuroinform.* 12:8. doi: 10.3389/fninf.2018.00008

The diversity of intrinsic dynamics observed in neurons may enhance the computations implemented in the circuit by enriching network-level emergent properties such as synchronization and phase locking. Large-scale spiking network models of entire brain regions offer a platform to test theories of neural computation and cognitive function, providing useful insights on information processing in the nervous system. However, a systematic in-depth investigation requires network simulations to capture the biological intrinsic diversity of individual neurons at a sufficient level of accuracy. The computationally efficient Izhikevich model can reproduce a wide range of neuronal behaviors qualitatively. Previous studies using optimization techniques, however, were less successful in quantitatively matching experimentally recorded voltage traces. In this article, we present an automated pipeline based on evolutionary algorithms to quantitatively reproduce features of various classes of neuronal spike patterns using the Izhikevich model. Employing experimental data from Hippocampome.org, a comprehensive knowledgebase of neuron types in the rodent hippocampus, we demonstrate that our approach reliably fit Izhikevich models to nine distinct classes of experimentally recorded spike patterns, including delayed spiking, spiking with adaptation, stuttering, and bursting. Importantly, by leveraging the parameter-exploration capabilities of evolutionary algorithms, and by representing qualitative spike pattern class definitions in the error landscape, our approach creates several suitable models for each neuron type, exhibiting appropriate feature variabilities among neurons. Moreover, we demonstrate the flexibility of our methodology by creating multi-compartment Izhikevich models for each neuron type in addition to single-point versions. Although the results presented here focus on hippocampal neuron types, the same strategy is broadly applicable to any neural systems.

Keywords: spiking model, compartmental model, hippocampal neurons, firing patterns, evolutionary algorithms

INTRODUCTION

In the last decade, several projects have built large-scale models of brain regions in an attempt to advance our understanding of how the nervous system functions (Izhikevich and Edelman, 2008; Eliasmith et al., 2012; Markram et al., 2015; Hendrickson et al., 2016). The biological realism in these models has been captured in varying levels of detail. One of the characterizing features of biological neural networks is the diversity observed in the intrinsic dynamics of individual neurons. This diversity likely contributes to the emergent properties of neural networks and, consequently, plays a major role in the information processing in the nervous system (Padmanabhan and Urban, 2010; Tripathy et al., 2013; Pozzorini et al., 2015). Therefore, a biologically realistic large-scale network model of a brain region should take into account intrinsic behavioral diversities both within and between neuron types.

Hippocampome.org is a comprehensive knowledgebase of 122 morphologically identified neuron types in the rodent hippocampal formation (Wheeler et al., 2015). One of the motivations behind developing this knowledgebase was to create a real-scale computational model of the entire hippocampus. Toward achieving this goal, we aim to create individual neuronal models using the electrophysiological and spike pattern properties of neuron types available at Hippocampome.org. In deciding which modeling system to use, we considered simulation costs. High simulation costs of biophysically detailed Hodgkin-Huxley-type neuronal models often impose limits on the scale of network models. Conversely, simpler models, such as leaky integrate-and-fire neurons, cannot capture the wide range of dynamics observed in the hippocampus. Models such as Izhikevich (Izhikevich, 2003) and Adaptive Exponential Integrate-and-Fire (AdEx) (Brette and Gerstner, 2005) have been shown to qualitatively reproduce various firing pattern classes observed experimentally in real neurons, while still being computationally efficient. Therefore, these simpler models with lower simulation costs allow large-scale modeling of biological neural networks in a computationally efficient manner. In this work, we create Izhikevich Models (IMs) that reproduce quantitatively comparable features of various hippocampal spike pattern classes through parameters optimization.

The dynamics of Izhikevich models are highly non-linear and error landscapes that are defined over the resulting parameter spaces typically exhibit properties that make them difficult to optimize, such as multiple local optima. As such, several studies have turned to non-convex, derivative-free optimization methods such as evolutionary algorithms (EAs) to fit a neuronal model's responses to experimentally recorded voltage traces. The models used in these studies range from simple spiking models such as AdEx (Rossant et al., 2010, 2011; Lynch and Houghton, 2015) to biophysically detailed Hodgkin-Huxley type models with multiple compartments (Gerken et al., 2005; Keren et al., 2005; Druckmann et al., 2007; Van Geit et al., 2007). Previous studies have also used various techniques such as a feature-based error function (Druckmann et al., 2007) and a phase plane trajectory density method (Van Geit et al., 2008) to create the error landscape for the EA search. Rössert

et al. (2016) created an approach to simplify morphologically detailed microcircuit models to their point-neuron counterparts by applying soma-synaptic correction (to account for dendritic attenuation and delay) and constraining Generalized Integrate-and-Fire neurons around an *in vivo*-like working point. Rounds et al. (2016) used EAs to match firing rates of IMs in a network to experimental recordings in the retrosplenial cortex. However, to our knowledge, optimization techniques have not been successfully used to fit intrinsic IM responses to experimental data. On benchmark optimization tests, the IM showed poor performance compared to other simple models (Rossant et al., 2010, 2011; Lynch and Houghton, 2015). This might be due to the failure to identify an appropriate EA configuration such as the choice of error function and variation operators that are well-suited for the IM parameter space.

Apart from its capability to quantitatively fit IM's responses to experimental voltage traces, the novelty of our automated modeling framework is the integration of spike pattern classification protocols. Previous work (Komendantov et al., in review) identified 23 distinct spike pattern classes overall, among the 89 morphologically distinct hippocampal neuron types in Hippocampome.org for which experimental recordings were available. A behavior for a certain neuron type was defined based on the set of all experimentally recorded spike patterns. If a neuron type exhibited spike patterns of more than one class under different experimental conditions (e.g., bursting and regular spiking for different current stimulation strengths), it was marked as a multi-behavior type. In contrast, a neuron type was marked as a single-behavior type, if all spike patterns recorded from the same neuron under different experimental conditions fell into the same qualitative class. Neuron types with only a single experimentally recorded spike pattern were also marked as single-behavior.

This article presents the modeling approach and results for single-behavior neuron types. We report at least one example for each of the nine distinct single-behavior types, with the goal of illustrating both the approach and the IM's ability to quantitatively reproduce a variety of neuronal behaviors observed in the hippocampus. The single behaviors reported here include spiking with and without frequency adaptation, delayed spiking, bursting, and intermittent spiking or stuttering. In addition to simple point-neuron (single-compartment) models, multi-compartment IMs were created, where the number of compartments varied from two to four depending on the dendritic invasion of a neuron type across hippocampal layers. For example, the somata of hippocampal pyramidal cells in the principal layer extend basal dendrites in the oriens layer and apical trees in the radiatum layer that reach to the lacunosum-moleculare. Thus, these neurons can be represented as 4 compartments, one for each layer (as illustrated in the Methods below). This stratification is important because it segregates the synaptic inputs: distal lacunosum-moleculare dendrites, for example, are the targets of entorhinal projections, while dendrites in radiatum receive intra-hippocampal connections. Although finer morphological variability observed across various neuron types may also contribute to network dynamics, compartmentalized dendritic

integration of distinct laminar inputs is likely to play a crucial computational role in cortical circuits. Furthermore, dendrites located in separate layers typically have different active and passive properties from each other and from the soma. A previous large-scale model of the thalamo-cortical system used multi-compartment IMs (Izhikevich and Edelman, 2008). However, that model did not capture the signal transmission properties between the dendrites and soma in a biologically accurate way. In addition, the dendritic compartments did not reflect the appropriate balance of active and passive properties. Another novelty of our automated modeling approach is its capability to create accurate dendritic representations in the multi-compartment IMs. Our dendritic compartments exhibit generally known active and passive properties of the dendrites of real neurons.

MATERIALS AND METHODS

In this article, a certain spike pattern class will be used to denote a neuron type's "behavior," since all the neuron types discussed here were examples of single-behavior types. It is worth mentioning that 14 of the 23 distinct spike pattern classes observed in the hippocampus are part of the multi-behavior types and, hence, not reported in this article. Modeling multi-behavior cases requires a different approach, which we are pursuing but remains beyond the scope of this article.

Spiking Model

We reproduced spike patterns by using the nine-parameter variant of the IM (Izhikevich, 2007) because we found that the EA could reliably find better solutions with this IM than the originally proposed four-parameter formalism. IMs have been shown to reproduce qualitatively many spike patterns observed in biological neurons. The state variables membrane voltage (V) and membrane recovery variable (U) govern this two-dimensional system. The recovery variable U approximates the channel kinetics of Hodgkin-Huxley type models (Hodgkin and Huxley, 1952), making it computationally much cheaper to simulate. Parameter " a " is the time constant for the recovery variable U . Parameter " b " defines the degree of coupling between the state variables V and U . Parameters " b " and " a " collectively determine whether the model is an integrator or resonator (Izhikevich, 2001). Parameters " V_{min} " and " d " are after-spike reset values for V and U , respectively. Parameter " k " defines the shape of the spike upstroke, and V_{peak} defines the spike cutoff value. Parameters V_r and V_t are resting and threshold voltages, respectively, and C is cell capacitance.

$$C \cdot \frac{dV}{dt} = k \cdot (V - V_r) \cdot (V - V_t) - U + I \quad (1)$$

$$\frac{dU}{dt} = a \cdot \{b \cdot (V - V_r) - U\} \quad (2)$$

$$\text{if } V = V_{peak} \text{ then } V = V_{min}, U = U + d$$

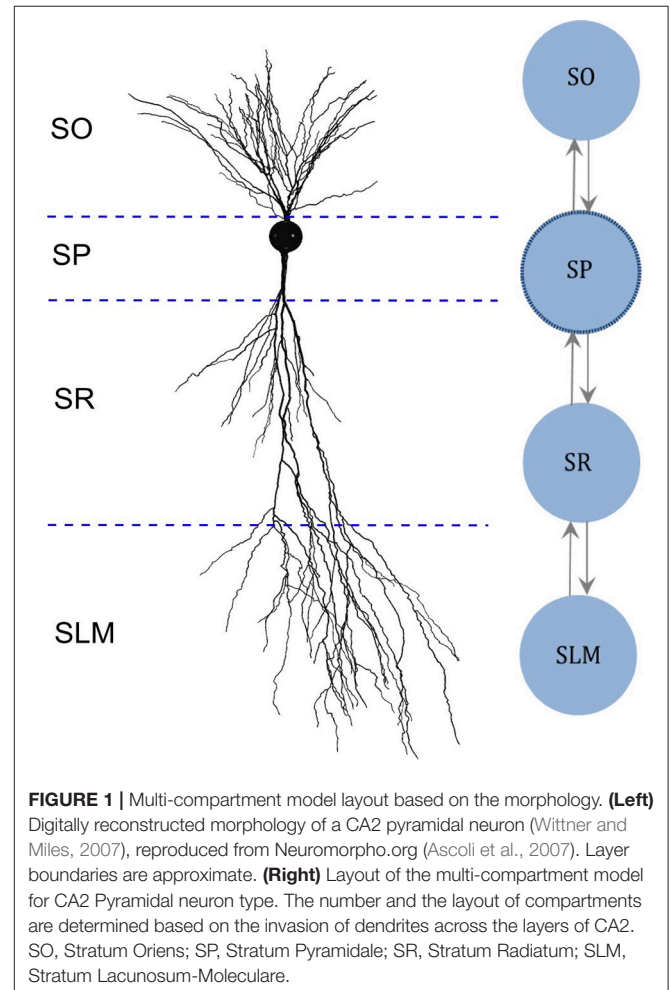
In addition, we created multi-compartment (MC) models for each neuron type based on the dendritic invasion across

the hippocampal layers (**Figure 1**), whereas each compartment represents the part of the dendritic tree present in a given layer. Compartments were coupled using an asymmetric mechanism. For example, the MC layout for the CA2 pyramidal neuron type depicted in **Figure 1** defines the compartment-specific coupling currents as follows:

$$I_{SP} = G_1 \cdot P_1 \cdot (V_{SP} - V_{SO}) + G_2 \cdot P_2 \cdot (V_{SP} - V_{SR}) \quad (3)$$

$$I_{SO} = G_1 \cdot (1 - P_1) \cdot (V_{SO} - V_{SP}) \quad (4)$$

Here, Stratum Pyramidale (SP) denotes somatic compartment, and Stratum Oriens (SO), Stratum Radiatum (SR) and Stratum Lacunosum-Moleculare (SLM) (**Figure 1**) are dendritic compartments. I_{SP} is the total coupling current at compartment SP , which results from the differences in the voltage between SP (V_{SP}) and SO (V_{SO}), and between SP and SR (V_{SR}). G_1 and G_2 are coupling constants, and P_1 and P_2 (with values between 0.01 and 0.99) determine the degree of asymmetry in the coupling, where a value of 0.5 denotes symmetric coupling.



Identification of Spike Pattern Classes

To classify the model behaviors, we used the same protocol developed for identifying various transient and steady-state elements of experimentally recorded spike patterns from the hippocampus (Komendantov et al., in review). Transient elements include: Delay (D), if the latency to spike is sufficiently long; Adapting Spiking (ASP), if the spike frequency decreases over time; Transient Stuttering (TSTUT), if a quiescent period follows a cluster of high frequency spikes; and Transient Slow-Wave Bursting (TSWB), if TSTUT is followed by a slow after-hyperpolarizing potential. Steady-state elements include: Silence (SLN), if the quiescence following the last spike is sufficiently long; Non-Adapting Spiking (NASP), if no spike frequency adaptation is identified in non-interrupted firing; Persistent Stuttering (PSTUT), if at least one sufficiently long quiescent period separates two clusters of high frequency spikes; and Persistent Slow-Wave Bursting (PSWB) if slow after-hyperpolarizing potential is present in an otherwise PSTUT pattern.

Given a sufficiently long duration of input current, transients will always be followed by a steady-state in a spike pattern. For example, ASP followed by NASP was identified in the spike pattern experimentally recorded from a CA3 Basket-CCK neuron (Gulyás et al., 2010) and this pattern is an instance of the class ASP.NASP (Figure 2A). The identified class of an experimentally recorded spike pattern represented the target class for model spike pattern. Thus, the criteria that defined a target class were used to validate the model behavior under the given input current. For details on the spike pattern classification criteria, see Komendantov et al. (in review) and Hippocampome.org¹

Evolutionary Optimization of Model Parameters

Many varieties of EAs exist along with numerous ways of implementing their specific components (De Jong, 2006). We employed a non-overlapping generational model of evolution and used elitism to ensure that the best individuals were always preserved in the population. In this section, we describe the specific components of the EA.

EA Configuration

Each individual in the evolutionary population consisted of a complete configuration of the IM we are seeking to tune. We represented these configurations as vectors of floating-points. During the search of the parameter space, we bounded each value within an allowed range. Choosing a biophysically reasonable range for each parameter up front has a significant effect on the efficiency of the optimization procedure, and through preliminary EA runs, we found that different behavior classes required slightly different ranges for some parameters.

When tuning a single-compartment model, each parameter vector contained $9 + n_I$ elements (genes), representing the 9 parameters of the IM ($k, a, b, d, C, V_r, V_t, V_{peak}, V_{min}$) and n_I input currents. n_I equaled the number of voltage traces (which

were recorded for different input currents) a model was fit to. A small range encompassing each experimentally injected input current ($I_{exp.}$), $[I_{exp.} - 10, I_{exp.} + 10]$ pA was included in the EA search. By allowing the EA to search within a small range, we boosted the exploration and identified more optimal points (across multiple EA trials) that are very similar in the phenotype. This design also helped to achieve more reliable fitting in cases where a single model was fit to multiple traces (see section Quantitative Comparison of Spike Pattern Features). In rare cases, where the experimental input current was unknown, an unbounded range of $[50, 800]$ pA was included for the search. The multi-compartment models had a larger number of parameters: if c is the number of compartments, we require $8c + 1$ parameters representing c compartments (the parameter V_r is the same for all c compartments), plus $2(c-1)$ parameters representing coupling parameters for consecutive compartment pairs, and n_I input currents.

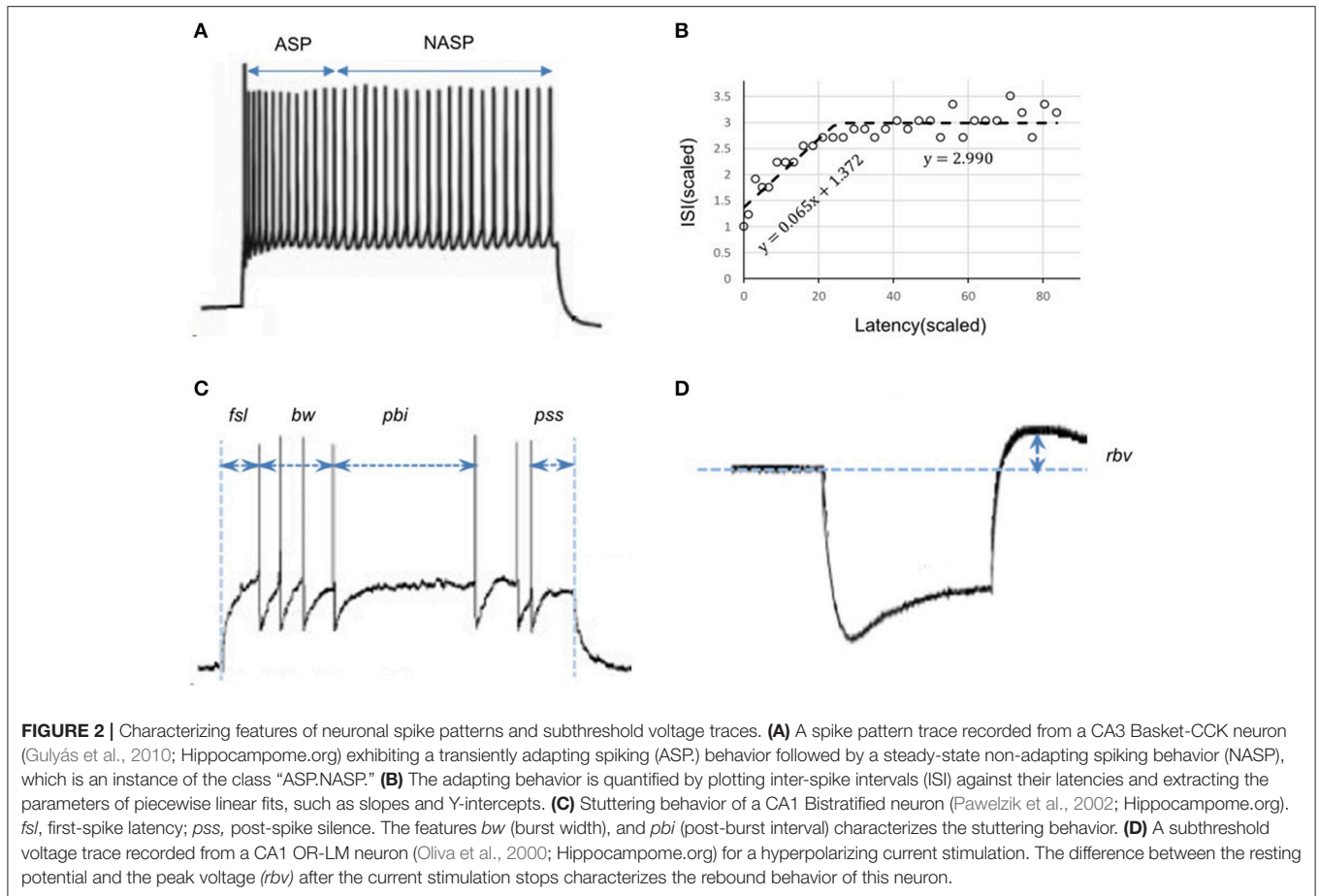
We first initialized a population of these vectors by sampling uniformly from within each parameter's allowed range. We used a fixed population size of 120 individuals for single-compartment IMs and of 400 for multi-compartment IMs. An exception was the 4-compartment ASP.SLN fast-spiking model, which we found was easier to optimize with a larger population size (800). After initializing the population, and at each generational cycle thereafter, we immediately selected the 10% of the population with the lowest error to survive to the next generation.

We filled the remainder of the child population by selecting parents via binary tournament and by applying two-point crossover and a mutation operator. Each gene had a probability of mutation between 0.1 and 0.3. For the parameters $d, C, G,$ and I , we applied an integer random-walk mutation: when selecting one of those genes for mutation, an integer increment or decrement was applied with equal probability. All remaining parameters were mutated by reset: a new floating-point value was randomly chosen out of that gene's allowed range. The EA was run until a maximum number of generations was reached. This number varied between 500 and 5,000 depending on the number of compartments in the model and the class of behavior the model was fit to.

Error Function

We employed a feature-based error function to quantitatively reproduce the spike pattern. Features for more than 250 experimentally recorded spike patterns are available at Hippocampome.org. These features include first-spike latency (fsl), post-spike silence (pss), spike frequency adaptation parameters (sfa), burst width (bw), post-burst interval (pbi), and rebound voltage amplitude (rbv) (Figure 2). Spike frequency adaptation (sfa) was quantified as previously detailed (Komendantov et al., in review) with a piecewise linear regression on the inter-spike intervals (ISIs) by extracting the parameters of linear fits such as slopes (m) and Y-intercepts (c) (Figure 2B). The error in the model sfa was calculated as follows: the two parameters of linear fit (for NASP and ASP. class) or three parameters of piecewise linear fits (for ASP.NASP class) obtained by plotting ISI's against their latencies to the second spike were compared between experimental and model spike patterns. In

¹http://hippocampome.org/php/Help_Principles_of_Classification_of_Firing_Pattern_Elements.php



addition, the number of ISIs (*nisi*) corresponding to a linear fit was also compared. For a bursting/stuttering class, the number of bursts (*nbs*) and the number of spikes (*nspikes*) within each burst were included.

Spike pattern classification protocols were also incorporated into the error function by dynamically assigning different weight factors to different features. This reduced the number of generations required for the EA to find an acceptable solution. In addition, for certain spike pattern classes, this approach more reliably found solutions across multiple stochastic trials. The error function was defined as:

$$error = \sum_{f \in S} (W_f \times \log(1 + |exp_f - model_f|)) \quad (5)$$

S : {*fsl*, *pss*, *m*, *c*, *nisi*} for continuous spiking, and S : {*fsl*, *pss*, *nbs*, *bw*, *pbi*, *nspikes*} for interrupted spiking (**Figure 2**).

Using the spike pattern classification protocols, the qualitative class of a candidate model's spike pattern was first identified. Then, the weight factor W_f was calculated for each feature by comparing the target class with the model spike pattern class. During the EA search, each feature weight changed based on that feature's distance from the target class boundary. These class boundaries are given by the set of criteria that define that class (see Supplementary Material section 1 for

pseudocode description of feature weight calculation). This accelerated the search during earlier generations of an EA, when many candidate solutions were outside the target class boundary (fast-exploitation toward narrow regions of interest). Once the population began converging within the target class boundary, this dynamic weight assignment scheme allowed slower exploration and ensured heterogeneity among the best models from within a class (see section Variabilities in the Intrinsic Properties within a Neuron Type).

In order to identify several possibilities, we ran a total of one thousand EA instances for each neuron type, yielding several best models due to the stochastic nature of the EA (different initial populations, stochasticity in variation operators, and selection pressure). At the end of an EA search, the best model was accepted only if its spike pattern class under the given input current matched the target class. If a single-compartment IM failed to reproduce a firing pattern class, two identical compartments were symmetrically coupled. We noticed that coupling effects enriched IM dynamics and were useful to reproduce certain subclasses of stuttering behavior (see Results section for examples).

The parameters of MC models were optimized such that the somatic compartment reproduced features of the experimentally recorded voltage traces both qualitatively and quantitatively using the same techniques discussed previously

for single-compartment models. Furthermore, four additional constraints were enforced in order to capture the known general active and passive properties of dendrites in the additional compartments. Unlike the somatic compartment constraints, all MC models shared the same dendritic constraints because of the lack of sufficient experimental dendritic voltage recordings. These general constraints include excitability and input resistance of dendrites relative to the soma as well as forward propagation of spikes and subthreshold signals.

Firstly, the dendritic compartments in MC models were constrained to be less excitable than the somatic compartment when they were decoupled. The minimum depolarizing current (I^{rheo}) required to elicit a spike at a compartment was used as the measure of its excitability (Aou et al., 1992). During the EA search, a ramp current rather than step currents was used to measure compartment excitabilities. This avoided the need for a local search for the minimum step current magnitude required to elicit a spike in each compartment. To reduce capacitive effects in measuring excitability, the ramp current had minimal slopes and high resolution of discrete increments (+0.1 pA/1 ms). Secondly, the decoupled dendritic compartments in MC models were constrained to have higher input resistances than the somatic compartment. The amplitudes of steady state voltage deflections from resting voltage (V^{def}) during a strong hyperpolarizing current input were compared between compartments to measure their relative input resistances. The spike propagation rate (R) was defined as the ratio between the number of spikes observed at the destination compartment and the number of spikes initiated at the source compartment. A few hundred excitatory synapses were stimulated at a dendritic compartment for spike initiation. On the other hand, a single AMPA synapse was stimulated at a dendritic compartment and the amplitude of the excitatory post-synaptic potential (EPSP) was measured at the somatic compartment. A range of (0.1, 0.9) mV was enforced for the EPSP amplitude. All synapses used a value of 10 for the weight, and this value is based on the range used for the multicompartment models by Izhikevich and Edelman (2008). The following errors were calculated for each dendritic compartment and added to the somatic spike pattern error described earlier:

$$error_{rheo} = \begin{cases} 0, & I_{dend}^{rheo} \geq I_{soma}^{rheo} \\ \log \left(1 + \left(I_{soma}^{rheo} - I_{dend}^{rheo} \right) \right), & I_{dend}^{rheo} < I_{soma}^{rheo} \end{cases} \quad (6)$$

$$error_{vdef} = \begin{cases} 0, & V_{dend}^{def} \geq V_{soma}^{def} \\ \log \left(1 + \left(V_{soma}^{def} - V_{dend}^{def} \right) \right), & V_{dend}^{def} < V_{soma}^{def} \end{cases} \quad (7)$$

$$error_R = \begin{cases} 0, & R = 1 \\ \log \left(1 + (1 - R) \right), & R < 1 \end{cases} \quad (8)$$

$$error_{eps} = \begin{cases} 0, & 0.1 \leq EPSP \leq 0.9 \\ \log \left(1 + (0.1 - EPSP) \right), & EPSP < 0.1 \\ \log \left(1 + (EPSP - 0.9) \right), & EPSP > 0.9 \end{cases} \quad (9)$$

Model and Algorithm Implementations

We used the open-source Java-based evolutionary computation system ECJ (Luke et al., 2015) to tune IM parameters. Single compartment models were simulated using the Apache

Commons Mathematics Library². The MC models with up to 39 open parameters were tuned using the parameter tuning interface of CARLsim, an open-source high performance GPU-based spiking neural network simulator (Beyeler et al., 2015). The EA and the single compartment model simulations were run on distributed CPU nodes, and the MC models were run on the GPU nodes available at the Office of Research Computing at George Mason University. All scripts necessary to reproduce the results reported in this article are publicly available³.

RESULTS

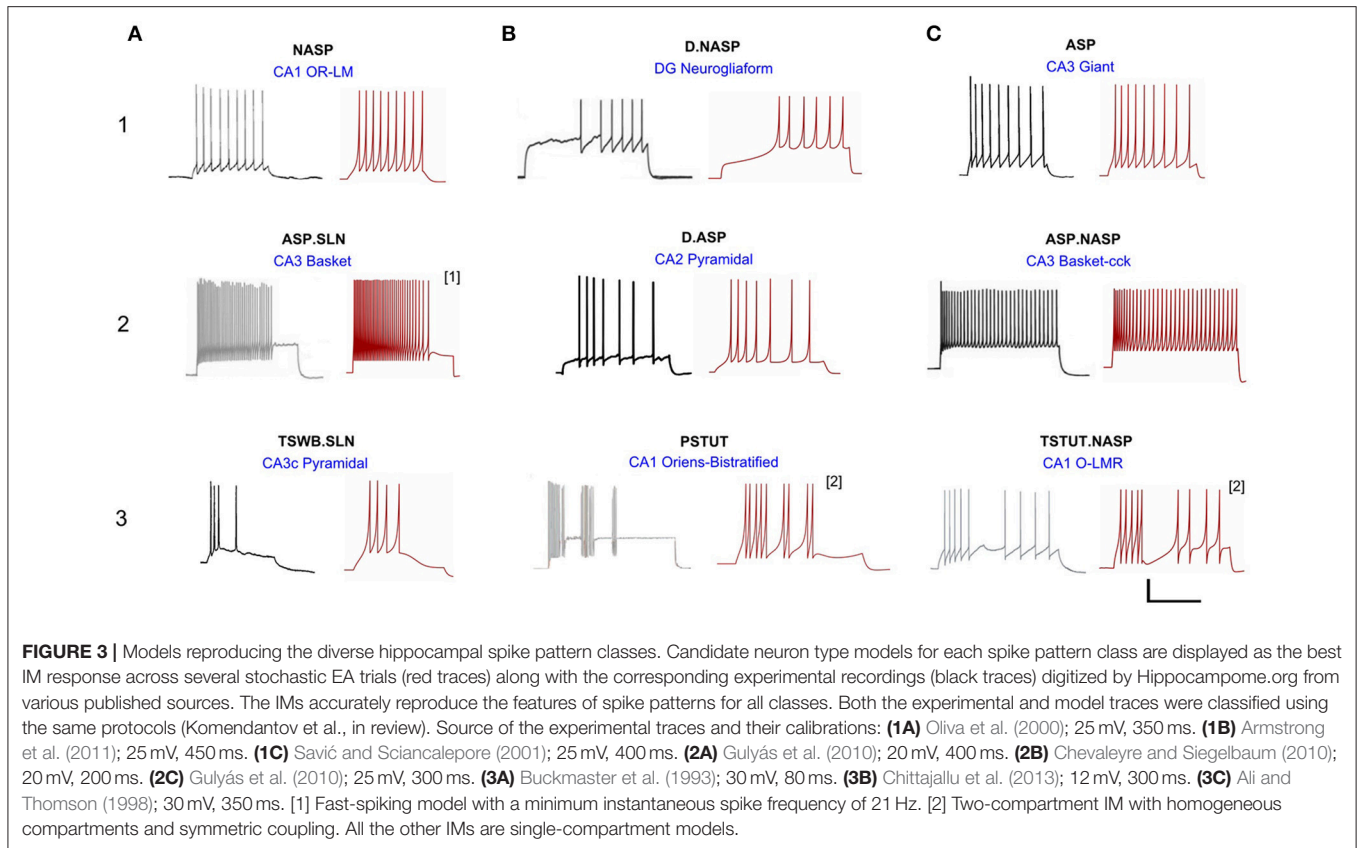
Models of Distinct Single Behavior Types

A total of 33 of 122 neuron types in Hippocampome.org version 1.0 (Wheeler et al., 2015) exhibit single behavior. Nine distinct single-behavior *classes* exist among these neuron types, and, in this article, we present at least one model for each of those classes. It is worth mentioning that different neuron types that exhibit the same qualitative behavior class typically exhibit different quantitative features and excitability levels. **Figure 3** illustrates an exemplar neuron type for each of the nine distinct single-behavior classes and the corresponding best model from all EA trials. Our simple models were able to reproduce quantitatively comparable spike pattern features for all these classes (see section Quantitative Comparison of Spike Pattern Features). While earlier models reproduced seven qualitatively different classes of spike patterns (Izhikevich, 2003), our models capture the spike pattern features of all observed single-behavior spike patterns in hippocampal neuron types both qualitatively and quantitatively. Importantly, our systematic and more detailed spike pattern classification identifies distinct hippocampal spike pattern classes within general firing behaviors (Komendantov et al., in review). For instance, among the adapting spike patterns, our approach distinguishes between the patterns that reach a specific steady state such as non-adapting or silence (ASP.NASP and ASP.SLN classes, respectively) and those with experimental recordings that only allow determination of the transient state (ASP. class). Our models effectively reproduced the features of these classes (**Figure 3**: ASP., ASP.SLN, and ASP.NASP).

All models shown in **Figure 3** are single compartment IMs except for PSTUT and TSTUT.NASP, which were reproduced by coupling two homogenous compartments. Although stuttering behavior can be modeled in a single compartment IM, multiple compartments (coupling effects) were required to accurately capture various subclasses of stuttering behavior such as TSTUT.NASP and TSTUT.ASP. However, the number of compartments for a multi-compartment IM is determined based on the neuronal morphology (see section Spiking Model) and CA1 O-LMR and CA1 Oriens-Bistratified neurons have both their soma and dendrites in the oriens layer. Thus, MC models were created by symmetrically coupling two identical compartments, unlike the MC IMs with morphologically defined layouts (section Constrained Multi-Compartment Models). These two-compartment IMs were able to capture the classes

²<http://commons.apache.org/proper/commons-math/>

³<https://github.com/Hippocampome-Org/Time>



PSTUT and TSTUT.NASP by integrating coupling effects into the IM dynamics. For the EA search, this simply means inclusion of an additional parameter (coupling constant). In many cases, the EA population converged in less than 500 generations, but certain classes required more generations (Figure 4). As mentioned in section Error Function, we reject the best solution found from a single EA run, if its spike pattern features do not meet the target class criteria (see section Diversity in the Intrinsic Properties across Neuron Types for discussion on the number of accepted models for different classes). The IM parameters of the nine models from Figure 3 are given in Table 1.

Quantitative Comparison of Spike Pattern Features

Our approach can reliably fit a model's responses to multiple experimental voltage traces. As an illustration, the model of a CA1 OR-LM neuron type (a variant of the O-LM interneuron superfamily with dendrites in oriens and axons in both radiatum and lacunosum-moleculare) was created by fitting its responses to four distinct experimental voltage traces recorded for different current stimulation strengths (Figure 5A). The model reproduces features of spike pattern and subthreshold voltage traces that are quantitatively comparable to the experimental traces (Table 2). The model spike pattern features are reported for the input currents that were selected by the EA (see Materials and Methods). In addition, only the minimum set of features required to fully capture the temporal properties of spike patterns

were included in the error function. For instance, single spike traces do not require *pss* as an objective feature, when *fsl* and *nspikes* are included. By allowing a narrow range for input current, the EA was able to reliably fit the model responses to multiple voltage traces. Although the voltage sag is not as clearly visible as in the hyperpolarized experimental trace, the corresponding model response nevertheless has a post-inhibitory rebound potential with a 7 mV amplitude. It should be noted that for multiple voltage trace fitting, we only considered traces that were recorded under the same experimental conditions (except for the strength of current stimulation), such as animal species (rat vs. mouse), electrode type (patch vs. sharp), and temperature (room vs. body). As mentioned in section Models of Distinct Single Behavior Types, our approach does not only differentiate between different classes of frequency adapting spike patterns, but also reproduces quantitatively comparable parameters of *sfa* (Figure 5B). See supplementary material (section Materials and Methods) for quantitative comparison between experimental and model traces for all nine classes from Figure 3.

Furthermore, our approach does not simply identify a single optimal point in the IM parameter space, but instead identifies several possibilities that correspond to the known behaviors of a certain neuron type. The size of such region of possibilities in the parameter space depends on the target behavior class to which the model is constrained as well as the amount of experimental data available for each neuron type. For instance, NASP behavior roughly correspond to the range (0.01, 0.1)

for the IM parameter “*a*,” whereas ASP., especially a strongly adapting behavior, significantly reduces the possibilities to the range (0, 0.005) for “*a*.” Similarly, if multiple experimental voltage traces were recorded for different input current strengths, the possibilities in the IM parameter space are reduced.

The variability in the quantitative features among all accepted models is given in **Figure 5C**. The experimentally observed feature typically lies within the range of features observed in the corresponding models, with few exceptions. For instance, while the IMs for the CA3 Giant neuron type exhibited a range of *sfa* slopes that encompassed the experimentally observed

sfa slope (**Figure 5C** bottom), its *fsi* lies outside the model range (**Figure 5C** top). These models were nonetheless accepted because they all satisfy the criteria for the target class (ASP.).

The best model for CA3 Basket (ASP.SLN) showed the highest error in the *sfa* slope among all the adapting classes (**Figure 5C** bottom). Yet, the accepted models for this neuron type not only exhibited the desired class (**Figure 3**, ASP.SLN), but also captured fast-spiking behavior, which plays an important role in network synchronization (Traub et al., 1996; Cardin et al., 2009). It should be emphasized that there is no guarantee that a model fit to a single experimentally recorded fast-spiking trace is indeed a fast-spiking model. For example, if the model of a CA3 Basket fast-spiking neuron type was created by simply fitting to the only available trace (**Figure 3**, ASP.SLN), it might still exhibit non-fast spiking behavior for a lower current input. To avoid this discrepancy, in fast-spiking models we enforced a minimum instantaneous frequency of 25 Hz for a step current close to the rheobase (**Figure 6**). In the end, a neuron type is represented by a set of heterogeneous models with similar behavioral features.

Constrained Multi-Compartment Models

In addition to the simple point-neuron models described in previous sections, we create MC Izhikevich models with heterogeneous compartments for all neuron types with dendrites spanning multiple hippocampal layers. These models capture the differences in the active and passive properties between soma and dendrites as well as coupling mechanisms that allow biologically realistic signal transmission between compartments. However, our MC models do not have branching dendritic arbors, and only consists of up to four compartments. This is because each additional compartment adds 10 new parameters for optimization, and tuning hundreds of compartments for each neuron type is an unrealistic goal. We assume that layer-level segregation of synaptic inputs is sufficient to significantly increase the computational power of the models in a network.

As an illustration, we present a four compartment model of CA2 pyramidal neuron type (**Figure 7**). The somatic compartment (SP) reproduced features of experimentally recorded voltage trace [see **Figure 3(2B)**] both qualitatively and quantitatively (**Figure 7A**). Furthermore, we enforced four additional constraints for MC models as detailed in section Error Function. Decoupled dendritic compartments are less

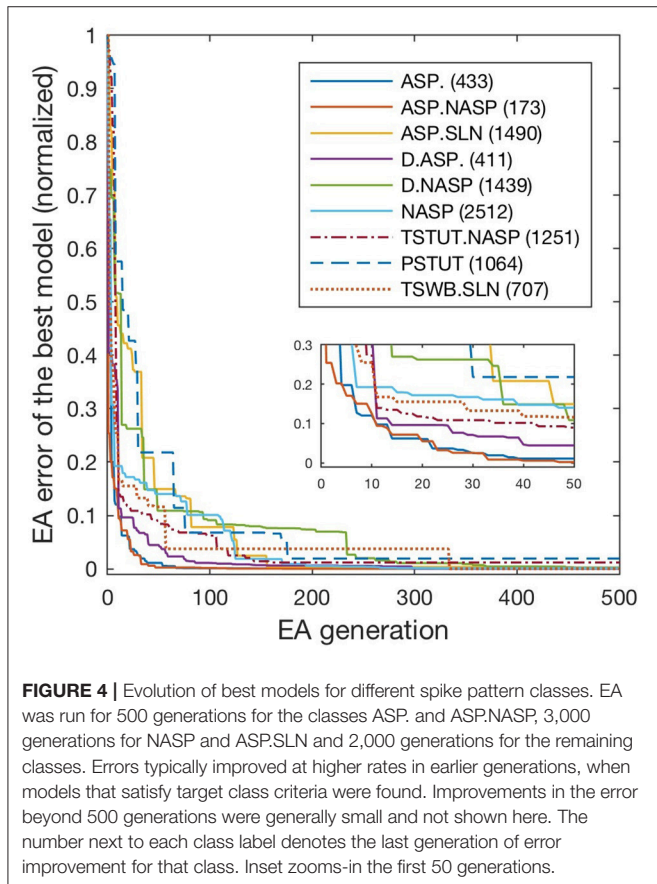
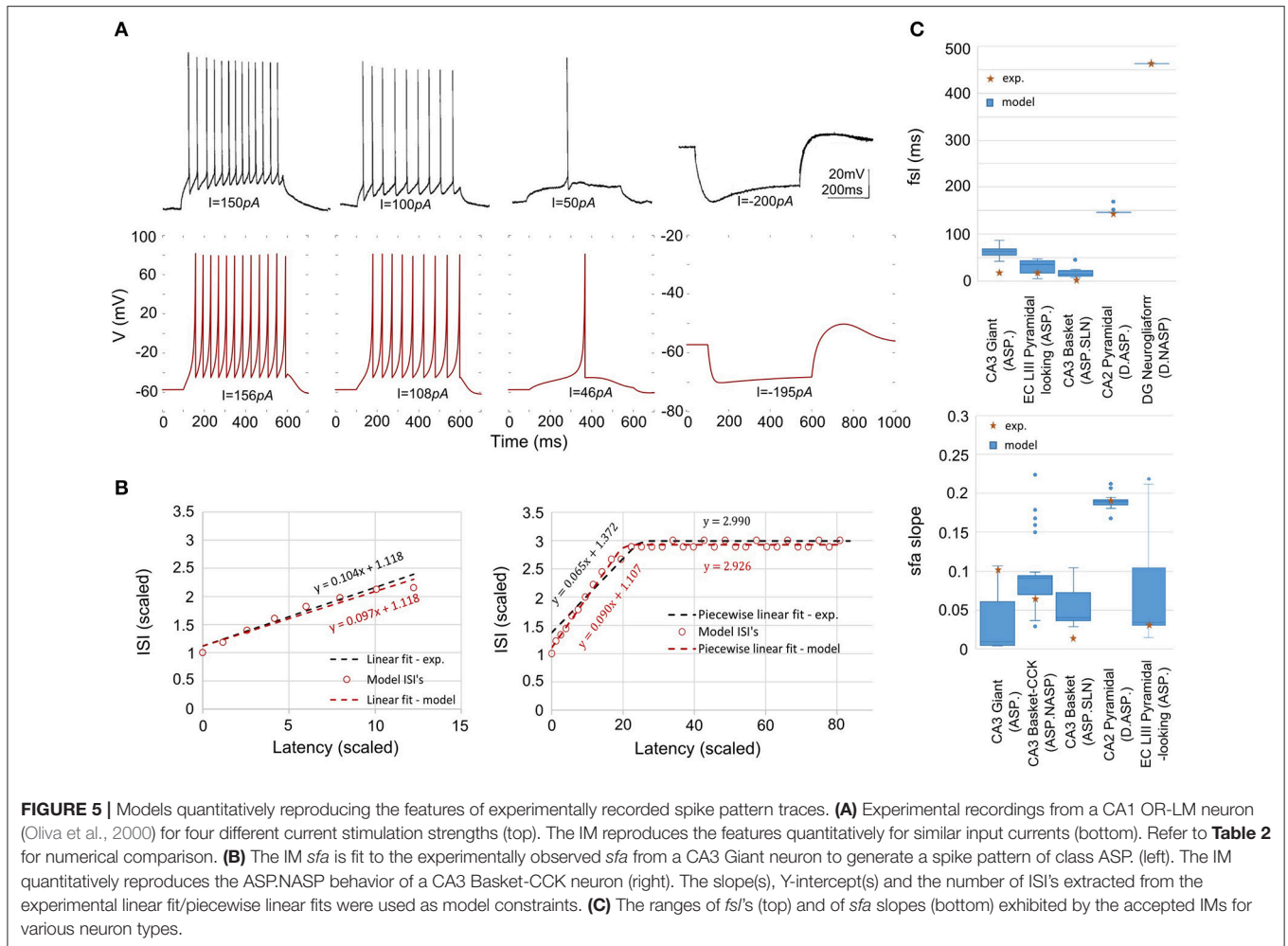


TABLE 1 | IM parameters for the nine models from **Figure 3**.

Neuron type	<i>k</i>	<i>A</i>	<i>b</i>	<i>d</i>	<i>C</i>	<i>V_r</i>	<i>V_t</i>	<i>V_{peak}</i>	<i>V_{min}</i>	<i>G</i>
CA1 OR-LM (NASP)	0.527	0.00223	6.15	-12	253	-57.25	-42.78	81.81	-44.97	-
DG Neurogliaform (D.NASP)	0.697	0.00107	-30.65	111	242	-74.15	-9.20	17.51	-39.44	-
CA3 Giant (ASP.)	0.609	0.00365	1.84	2	96	-57.58	-37.12	36.42	-49.45	-
CA3 Basket (ASP.SLN)	0.995	0.00385	9.26	-6	45	-57.28	-23.16	18.68	-47.33	-
CA3 Basket-CCK (ASP.NASP)	0.583	0.00574	-1.24	54	135	-59.00	-39.40	18.27	-42.77	-
CA2 Pyramidal (D.ASP.)	5.943	0.00114	-15.89	74	1630	-72.59	-58.78	19.99	-62.65	-
CA1 O-LMR (TSTUT.NASP)	0.326	0.00632	0.40	48	96	-56.44	-27.62	29.48	-51.29	12.00
CA3c Pyramidal (TSWB.SLN)	3.006	0.00189	19.36	104	244	-62.29	-45.27	17.43	-47.37	-
CA1 Oriens-Bistratified (PSTUT)	2.91	0.00168	13.67	35	841	-57.11	-48.50	4.12	-52.94	67.00



excitable than the somatic compartment (**Figure 7B**) and have higher input resistances (**Figure 7C**). It should be noted that the dendritic input resistances and excitabilities were only enforced qualitatively (the quality of being higher or lower) relative to the somatic compartment. Neither the absolute values nor the magnitudes of the differences were enforced in the error function (see Equations 6 and 7 in section Error Function).

In addition, the dendritic compartments allow forward propagation of spikes to the adjacent compartments. A few hundred excitatory synapses were simultaneously stimulated in order to initiate a spike at a dendritic compartment, and forward spike propagation (in the direction toward soma) was verified at the adjacent compartment (**Figure 7D**). Interestingly, the SLM compartment required an additional depolarizing current of 1,200 pA in order to initiate a spike, consistent with experimental observations (Jarsky et al., 2005). Although we enforced a spike propagation rate of 1 for isolated spikes initiated at a dendritic compartment (see section Error Function), we noticed that the rate was less than 1 for high frequency dendritic spike trains. Finally, the amplitude of unitary EPSP measured at the somatic compartment was constrained to be in the biologically realistic range of (0.1, 0.9) mV (**Figure 7E**).

Even though not directly enforced in the error function, our MC models qualitatively exhibited the known directional voltage attenuation properties of hippocampal neurons: voltage attenuation from a dendritic location to the soma is much higher than in the opposite direction (Mainen et al., 1996; Carnevale et al., 1997; Chitwood et al., 1999; Golding et al., 2005). This behavior was observed in the models because of the higher input resistances of the dendritic compartments and the asymmetric coupling between the compartments. The EA always selected weaker coupling toward the soma than away from it. Optimization of a 4-compartment model required ~ 20 h of total execution time on the GPU. This is roughly a 15X speedup from CPU execution. The 39 parameters of the model from **Figure 7** are given in **Table 3**.

Variabilities in the Intrinsic Properties Within a Neuron Type

Our models of hippocampal neuron types were constrained using voltage traces digitized from figures in the published literature. It is thus natural to ask: how faithfully does a representative recording from a single neuron, which the authors chose to include in an article, reveal the real intrinsic property of

TABLE 2 | Quantitative comparison of spike pattern features between experimental and model traces of the CA1 OR-LM neuron type given in **Figure 5A**.

Exp.	<i>I</i>	150 pA	100 pA	50 pA	−200 pA
<i>fsl</i>		40.1 ms	30.39 ms	200 ms	–
<i>pss</i>		18.38 ms	7.31 ms	–	–
<i>sfa</i> :	<i>c</i>	1.176	1.196	–	–
	<i>nISI</i>	12	8	–	–
<i>rbV</i>		–	–	–	7 mV
<i>nSpikes</i>		–	–	1	–
Model	<i>I</i>	156 pA	108 pA	46 pA	−195 pA
<i>fsl</i>		58.9 ms	79.9 ms	268 ms	–
<i>pss</i>		8.9 ms	3.1 ms	–	–
<i>sfa</i> :	<i>c</i>	1.176	1.198	–	–
	<i>nISI</i>	11	8	–	–
<i>rbV</i>		–	–	–	7 mV
<i>nSpikes</i>		–	–	1	–

that neuron type? Under the same experimental conditions, a different neuron of the same type might behave slightly differently due to experimental noise and biological variability. A truly accurate model of a neuron type should take into account (and even represent) such intra-neuron type behavioral variabilities. For instance, if the experimental data consist of spike pattern traces recorded from several neurons of the same type under the same experimental conditions, the error function could use statistical measures such as z-score to capture the variability in the models (Druckmann et al., 2007; Markram et al., 2015). However, we ultimately strive to create spiking models for over a hundred hippocampal neuron types based on the available experimental data as gleaned in Hippocampome.org. Except for a few well-studied neuron types such as CA1 pyramidal neurons, DG granule neurons, and a handful of GABAergic interneurons, the vast majority of neuron types identified in the hippocampal formation to date lack adequate data to represent their behavioral variabilities. While such a paucity of empirical evidence might pose the risk of overfitting the model to experimental noise, two key aspects of our approach synergistically reduce that risk: (i) inclusion of qualitative class criteria in the error function and (ii) parameter space exploration using the EA.

Firstly, we dynamically weigh the feature errors during the EA search with weights determined by comparing the model's spike pattern class to the experimental target (see section Materials and Methods). This ensures that several near-optimal points in the error landscape represent the appropriate class, even though the exact feature errors might be higher than the globally optimal point (**Figure 8A**). Without such a weight-assignment scheme, a near-optimal point might not necessarily represent the target class, because both the feature that defines a boundary between classes (e.g., *fsl* between ASP. and D.ASP.) and the feature that does not (e.g., *pss* between ASP. and D.ASP.) would equally contribute to the error. Thus, explicitly integrating qualitative

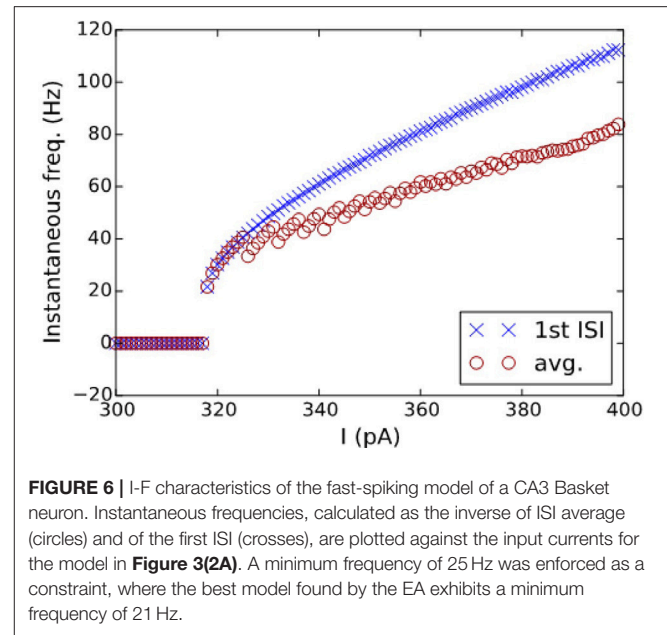


FIGURE 6 | I-F characteristics of the fast-spiking model of a CA3 Basket neuron. Instantaneous frequencies, calculated as the inverse of ISI average (circles) and of the first ISI (crosses), are plotted against the input currents for the model in **Figure 3(2A)**. A minimum frequency of 25 Hz was enforced as a constraint, where the best model found by the EA exhibits a minimum frequency of 21 Hz.

definitions in the error function sharply distinguishes the near-optimal points that satisfy class criteria from the ones that do not (**Figure 8B**). This increases the EA's chances of finding the models that reproduce the target class.

Secondly, rather than just exploiting the search space to identify a single optimal point that precisely reproduces the spike times, our approach explores the search space and identifies numerous points that elicit a similar behavior. The similarity is governed by the qualitative class definitions, which are inherent to the error landscape as described before. The EA exploration was boosted by a high-rate reset mutation along with a two-point crossover. The downside of such a configuration is the reduced EA reliability in finding acceptable models in certain cases. For instance, only 651 out of 1,000 trials found best models that satisfy the target class criteria (ASP.) for the CA3 Giant neuron type (**Figure 8B**). It is possible to increase this EA reliability by using a step mutation with a lower rate; however, this will be achieved at the cost of global exploration, ultimately resulting in reduced heterogeneity in the accepted models. In the end, a subset of all best models exhibiting quantitative features with a certain degree of variability is chosen to represent a neuron type (section Quantitative Comparison of Spike Pattern Features). Those features strictly adhere to the criteria for the qualitative class of the spike pattern recorded from that neuron type.

There is no guarantee to avoid over-fitting the best model from a single EA trial to the experimental noise. However, by reducing the acceleration of evolution within the bounds of target class (dynamic feature weight assignment), and identifying several near-optimal points within these bounds (parameter space exploration), we reduce the risk of the best models from all EA trials converging to a single globally optimal point, which might or might not represent a noisy feature. It is worth remembering that a feature threshold of a spike pattern class was

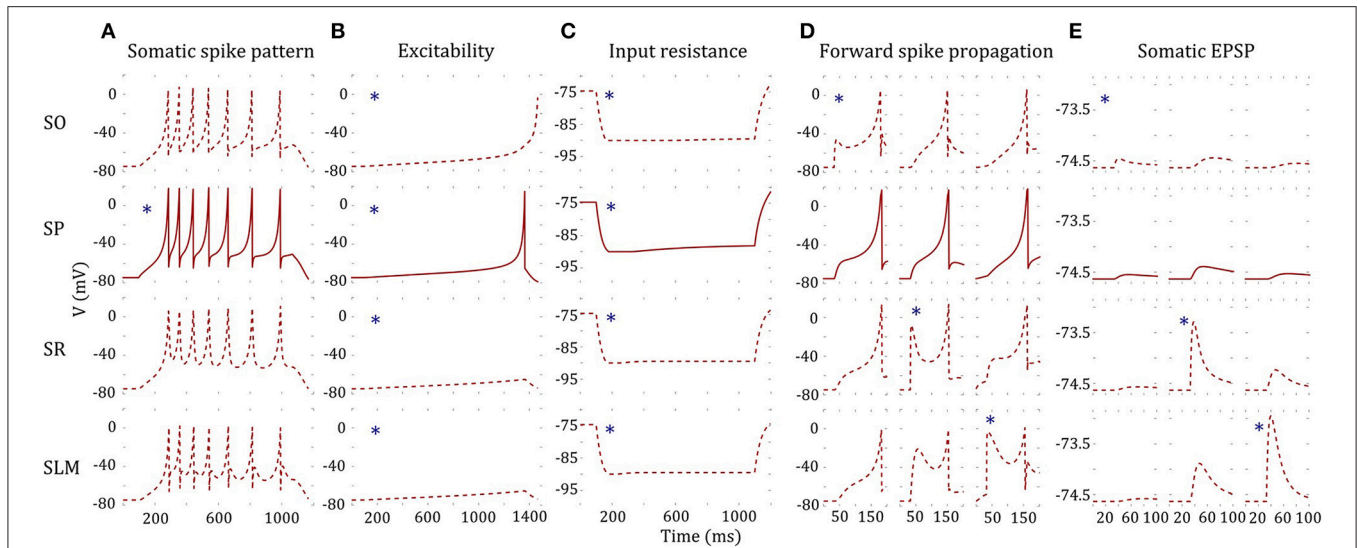


FIGURE 7 | A four-compartment model of a CA2 Pyramidal neuron. *indicates stimulated compartment (using input current/excitatory synapses) **(A)** Somatic compartment reproduces spike pattern of class D.ASP. for $I = 401 \text{ pA}$ with $f_{SI} = 188 \text{ ms}$, $s_{fa} = y = 0.173x + 1.017$ [compare with experimental trace in **Figure 3(2B)** and features in **Figure 5C**]. **(B)** Decoupled dendritic compartments (DC) are less excitable than the somatic compartment (SC). SC spikes before DC's for ramp current (ramp slope: 0.1 pA/1 ms). **(C)** Decoupled DC's have higher input resistance (IR) than the SC. IR is measured by the steady state voltage deflection due to a hyperpolarizing current application (-500 pA). The amplitudes of voltage deflections are 14.92, 13.66, 14.83, and 14.87 mV for SO, SP, SR, and SLM, respectively. **(D)** The model and coupling parameters were optimized to enable forward propagation of spikes to the adjacent compartment. A total of 200 excitatory synapses were stimulated at 40 ms to initiate a spike at a DC. The SLM compartment required an additional input current of $1,200 \text{ pA}$ to elicit a spike. Only the forward spike propagation was enforced. **(E)** The model was constrained to evoke a unitary EPSP with amplitude in the range (0.1, 0.9) mV. Excitatory synapses were stimulated at SO, SR, and SLM, and the amplitude of the EPSP was measured at SP. EPSP amplitudes at SP were 0.09, 0.24, and 0.1 mV by stimulating a single synapse at SO, SR, and SLM, respectively.

TABLE 3 | IM parameters of the 4-compartment model from **Figure 7**.

Compartment	<i>k</i>	<i>A</i>	<i>b</i>	<i>d</i>	<i>C</i>	<i>V_r</i>	<i>V_t</i>	<i>V_{peak}</i>	<i>V_{min}</i>	<i>G</i>	<i>P</i>
SO	0.875	0.004	9.154	41	1163	-74.633	-61.327	7.440	-66.761	170	0.407
SP	1.029	0.002	11.054	40	1164	-74.633	-62.009	18.314	-65.184	-	-
SR	0.840	0.016	10.912	42	1174	-74.633	-62.307	14.142	-63.394	169	0.169
SLM	0.833	0.019	9.471	42	1170	-74.633	-60.468	2.444	-66.223	169	0.348

statistically inferred from the distribution of that feature from all neuron types (Komendantov et al., in review).

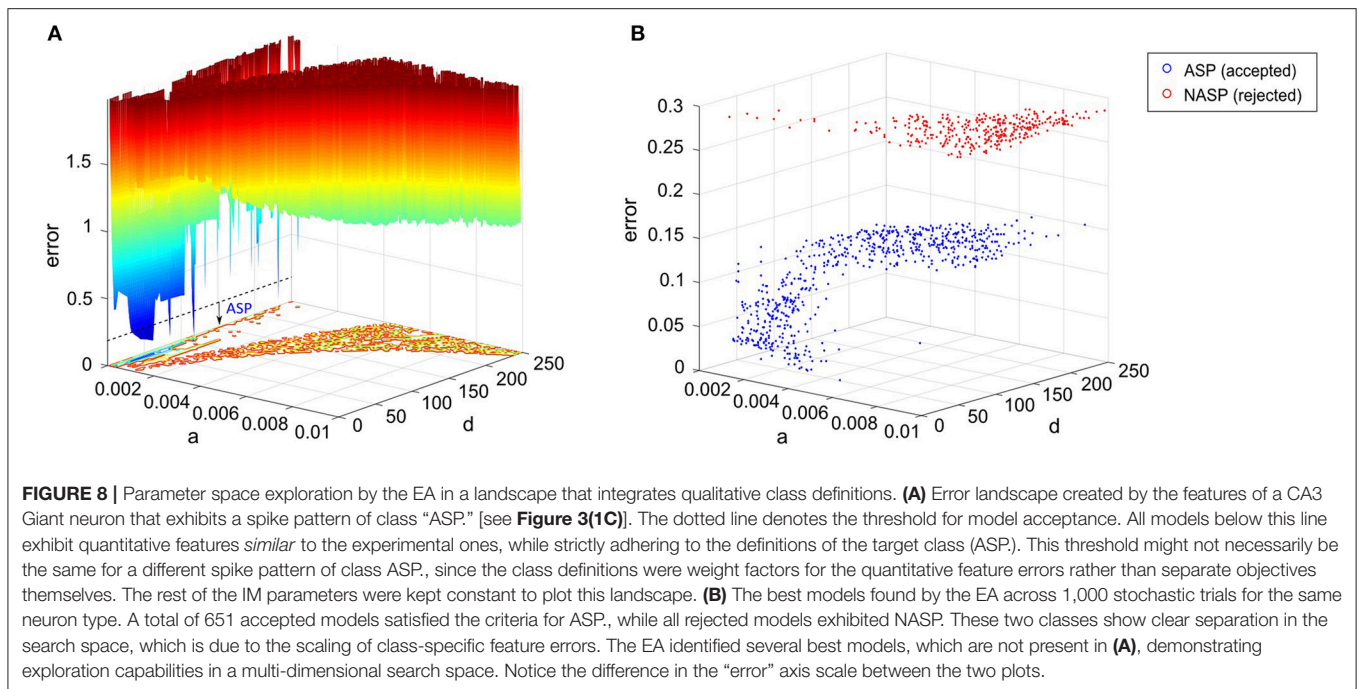
The accepted models for a single behavior showed notable variation in their parameters, except for TSTUT.NASP (**Figure 9A**). Such a variation was most prominent for parameters “*a*,” “*b*,” and “*d*,” but only the dimensions “*a*” and “*b*” are shown in **Figure 9A** for the nine single-behavior types. Thus, a wide range of parameters yielded similar behaviors, demonstrating the robustness of our EA in exploring the parameter space. This is also consistent with the notion that a given neuron behavior may result from multiple distinct combinations of ion-channel conductance densities (Marder and Prinz, 2002).

Diversity in the Intrinsic Properties Across Neuron Types

In section Variabilities in the Intrinsic Properties within a Neuron Type, we discussed within-neuron type variabilities, where several IMs for a single neuron type reveal slightly different quantitative features for similar input currents. In addition

to this, feature diversities across different neuron types, both qualitative and quantitative, also likely play a major role in the emergent properties in a network.

Even different neuron types that exhibit similar qualitative behavior might reveal substantial diversity in their quantitative features. For instance, the neuron types that include transient ASP. in their behavior are CA3 Giant (ASP.), CA3 Basket CCK (ASP.NASP), CA3 Basket (ASP.SLN), and CA2 Pyramidal (D.ASP.). The magnitudes of *sfa* experimentally observed from these neuron types were ~ 0.1 for 100 pA , ~ 0.06 for 400 pA , ~ 0.02 for 400 pA , and ~ 0.2 for 400 pA , respectively (**Figure 5C**). The IMs constrained using these features reveal considerable diversity in the magnitudes of *sfa* among these four models when the input current is gradually increased, as evidenced by plotting *sfa* against a range of input currents “*I*” (**Figure 9B**). For all cases, *sfa* decreased exponentially with linear increases of “*I*.” However, these models showed notable differences in their excitabilities and their *sfa* ranges. Most of the variance in *sfa* slopes for the fast spiking CA3 Basket PV+ model could



be explained by a narrow range of inputs (325–425 pA). This window is much larger for the regular spiking CA2 pyramidal model. **Figure 9B** illustrates the diversity of input-dependent *sfa* ranges among these four models. Although experimental data are too sparse to validate such ranges of *sfas* in the models, the above results demonstrate that our approach can create models with remarkable quantitative diversities, even with limited amounts of data.

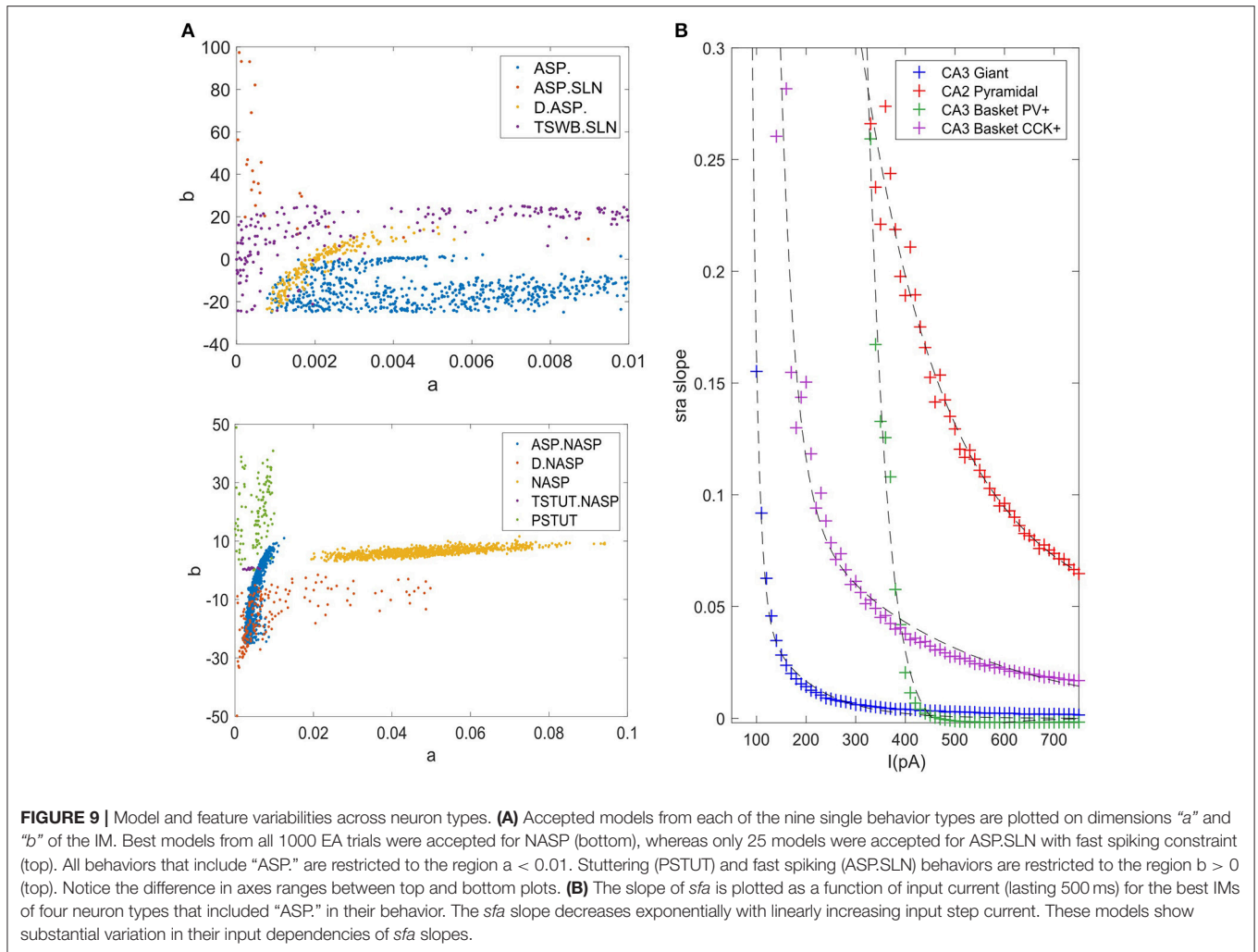
The diverse single behavior classes were most separated along the dimensions “*a*” and “*b*” of the parameter space (**Figure 9A**). The four behaviors that include ASP. were restricted to very small values of “*a*” (<0.01), whereas the NASP models converged to a broad range (0.02, 0.1). As mentioned in section Spiking Model, “*a*” is the time constant for recovery variable “*U*,” and lower values for “*a*” results in stronger *sfa*. The region “*b*” > “*a*” correspond to Andronov-Hopf bifurcation (Izhikevich, 2003) and all the fast-spiking ASP.SLN models were identified in the range (9, 90) for “*b*”. Although only 25 best models from 1,000 EA trials satisfied the criteria for ASP.SLN and fast-spiking, these models encompassed a broad range for “*b*” (**Figure 9A** top).

The optimal region for each class is shown in **Figure 10**. There is a significant overlap between the regions for the classes ASP. and ASP.NASP (see also **Figure 9A**). This is because the difference between these two classes often depends on the input conditions rather than the nine parameters of the model. It is worth mentioning again that in the ASP. class only the transient element is present in the spike pattern. Given a longer duration of input, this pattern will most likely show a steady-state of NASP. The classes NASP and D.NASP encompassed larger regions in the parameter space (**Figures 9A, 10**). In the case of D.NASP, this is likely due to the fact that the experimentally injected input current was unknown (see Supplementary Table A1), and the EA

identified several possibilities for similar behavior under a broad range of input currents.

DISCUSSION

A major motivation behind the current work is the intent to create large-scale network models using IMs with both biologically realistic within-neuron type behavioral variabilities and experimentally validated between-neuron type diversity. Our compact model representations of diverse neuron behaviors allow the implementation of hippocampal circuit simulations in a computationally efficient manner. More importantly, our results offer a sampling range for a neuron group in a network model (**Figures 9A, 10**). Several studies have shown that neurons have intrinsic plasticity and undergo homeostatic regulatory mechanisms, which modify their non-synaptic ion-channels such as sodium and delayed-rectifier potassium channels, in order to maintain a certain target activity level in the network (Desai et al., 1999; Aizenman and Linden, 2000; Desai, 2003). This implies similar intrinsic properties or behaviors can arise from various combinations of ion channel conductance densities (Foster and Ungar, 1993; Marder and Goaillard, 2006; Schulz et al., 2006). In the mathematically abstracted IM, this is equivalent to various combinations of parameter interactions. Although it might be difficult to describe such interactions mathematically, a robust EA can identify several optimal points in the multi-dimensional search space that correspond to the known behaviors of a neuron type (**Figure 8B**). Thus, our method represents a neuron type as possibilities in the model parameter space (**Figure 9A**). Such a representation is crucial for a thorough and systematic investigation of the contributions of neuronal intrinsic properties to network behavior and function. Our multi-compartment



models extend this platform to investigate the effects of dendritic filtering on the emergent network properties, while still being reasonably compact.

Furthermore, the diversity captured in our models may help experimentalists identify and distinguish real neurons in finer electrophysiological terms. Our models of *sfa* suggest the existence of different critical input windows for different neuron types as explained in section Diversity in the Intrinsic Properties Across Neuron Types (**Figure 9B**). Thus, a neuron exhibiting *sfa* could be characterized by the range of *sfa* slopes and its critical input window. The *sfa* makes a neuron act as high-pass filter (Benda and Herz, 2003) and plays a role in emergent network synchronization (Ermentrout et al., 2001). Two neurons with different input-dependent *sfa* ranges will likely have different filtering properties, and consequently, may contribute to network synchronization in different ways.

An advantage of using a Pareto-optimal front approach for model optimization (Druckmann et al., 2007) is that it avoids the need to weigh different feature errors. However, the performance of such multi-objective optimization techniques is affected by the number of objectives (Khare et al., 2003)

and exponentially increasing population sizes are required to represent high-dimensional Pareto-optimal fronts (Deb, 2014). A single interrupted spike pattern trace (e.g., TSTUT.NASP in **Figure 3**) presents at least eight objectives for optimization (see Supplementary Table A2, CA1 O-LMR). Moreover, some of our simple models are constrained using several spike pattern traces (**Figure 5A**). With population sizes as small as 120, our approach can efficiently optimize model parameters for several objectives.

On the other hand, the approach created by Rössert et al. (2016) requires a data-driven microcircuit model constructed from morphologically detailed neuron models (such as the one in Markram et al., 2015) as a reference, and such reference models are computationally very expensive. Compared to this approach, our simple models might be less constrained in some cases, but they significantly reduce the open parameter space size to create biologically accurate circuit models. Furthermore, our simplified multi-compartment models intrinsically capture the dendritic voltage attenuation properties without a need for synaptic correction (section Constrained Multi-Compartment Models).

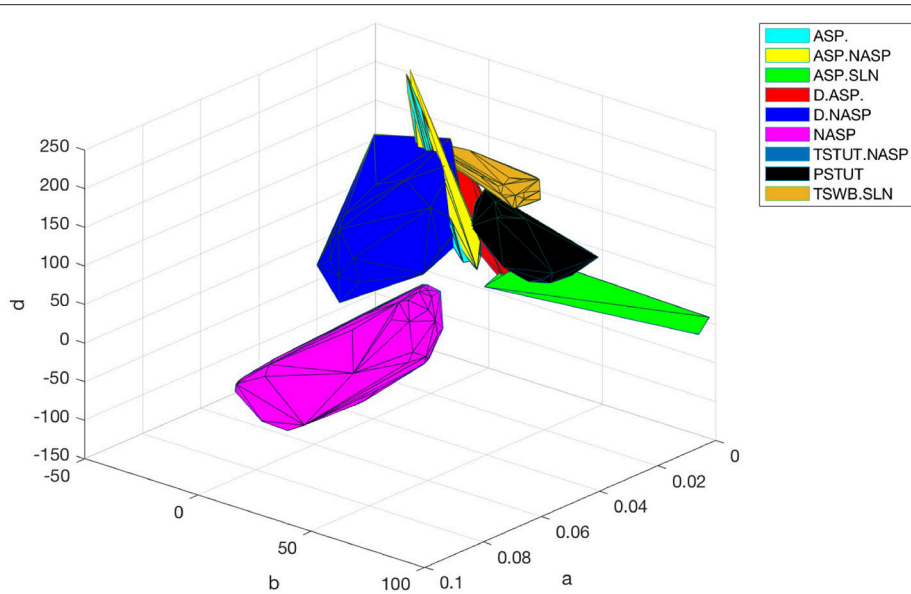


FIGURE 10 | Optimal regions of different spike pattern classes. Region for a class was obtained by plotting the convex hull from all the accepted models. The relationship between parameters “a” and “b” determines the type of bifurcation and it separates several classes. There is significant overlap between the classes ASP and ASP.NASP. In general, the EA identified a wide range of optimal points for each class along the dimensions “a,” “b,” and “d”. The classes NASP and D.NASP encompassed larger regions than other classes. The region for TSTUT.NASP, which lies very close to PSTUT (see **Figure 9A**–bottom) is the smallest region and is not visible here.

The precise shape of the spike was not captured in some of our models (for example, D.NASP in **Figure 3**). This could be attributed to the quadratic voltage dependence in the IM voltage equation. The AdEx model (Brette and Gerstner, 2005), which replaces the quadratic term in the IM with an exponential term for the voltage dependence, has been shown to reproduce more realistic spike shapes (Badel et al., 2008). However, our selection criteria for the models were entirely based on the temporal features of the overall spike pattern, and do not include characteristics of individual spikes. More important for the information processing in a neural network are the excitability of neurons, the precise timing of spikes, and the properties of connections. The shape of the spike is unlikely to play an equally prominent role in network dynamics. In fact, in the nine-parameter IM formalism “ k ” and “ V_t ” collectively determine the shape of the spike. It is thus possible to obtain realistic spike shape by restricting the ranges for these parameters (e.g., **Figure 3**, ASP.SLN). However, we did not explore these parameter ranges and interactions for all the cases for the reasons mentioned above.

Although only IMs have been presented in this article, our framework can be easily enhanced to include any phenomenologically rich model of spiking behavior. The only part of this framework that is specific to the IM is the EA configuration presented in section EA Configuration. This configuration was identified partly based on the topographical features of error landscape created by the IM parameters. Once an appropriate EA configuration is identified, our error function and spike pattern classification procedures are readily applicable to any alternative model.

In the future, we will enhance our framework to model multi-behavior neuron types. At least 15 morphological neuron types in the Hippocampome.org exhibit sharply distinguishable qualitative features under different experimental conditions. One of the commonly occurring multi-behavior types in the hippocampus is stuttering and spiking observed in a single neuron for different current stimulation strengths. For example, a CA1 Bistratified neuron exhibited stuttering and regular spiking behaviors for 400 and 600 pA, respectively (Pawelzik et al., 2002). Similarly, a CA1 Neurogliaform projecting neuron exhibited this multi-behavior for 500 and 700 pA (Price et al., 2005). Our preliminary work with multi-behavior types revealed vast possibilities for modeling such behaviors using IM, which could also provide insights into the existence of electrophysiological subtypes for a given morphological type.

The categorization of neuron type behaviors as either single-behavior or multi-behavior is solely based on the currently available experimental data. Consequently, it is possible that additional qualitative behaviors will be observed in future experiments from neuron type currently considered to display a single-behavior based on available data. An advantage of our modeling approach is that it identifies many possibilities for the known behaviors of a neuron type in the IM parameter space. Furthermore, the flexibility of our framework allows easier addition of newly observed behaviors from a neuron type to improve the accuracy of its model representations. Eventually, we plan to create models for over a hundred hippocampal neuron types and to make them freely available at Hippocampome.org. Nevertheless, although the modeling framework and the results presented in this article pertain to the hippocampus,

our approach could be easily adapted to other brain regions.

AUTHOR CONTRIBUTIONS

SV, AK, and GA created the overall approach and all the models. SL and JK extended the CARLsim framework to include simulation of multicompartment Izhikevich models on the GPU. ES and KD developed the interface between ECJ and CARLsim.

FUNDING

This work is supported by grants R01NS39600 (NIH) and IIS-1302256 (NSF). Publication of this article was funded in part by

REFERENCES

- Aizenman, C. D., and Linden, D. J. (2000). Rapid, synaptically driven increases in the intrinsic excitability of cerebellar deep nuclear neurons. *Nat. Neurosci.* 3, 109–111. doi: 10.1038/72049
- Ali, A. B., and Thomson, A. M. (1998). Facilitating pyramid to horizontal oriens alveus interneurone inputs: dual intracellular recordings in slices of rat hippocampus. *J. Physiol.* 507, 185–199. doi: 10.1111/j.1469-7793.1998.185bu.x
- Aou, S., Woody, C. D., and Birt, D. (1992). Increases in excitability of neurons of the motor cortex of cats after rapid acquisition of eye blink conditioning. *J. Neurosci.* 12, 560–569.
- Armstrong, C., Szabadics, J., Tamás, G., and Soltesz, I. (2011). Neurogliaform cells in the molecular layer of the dentate gyrus as feed-forward γ -aminobutyric acidergic modulators of entorhinal–hippocampal interplay. *J. Comp. Neurol.* 519, 1476–1491. doi: 10.1002/cne.22577
- Ascoli, G. A., Donohue, D. E., and Halavi, M. (2007). NeuroMorpho.Org: a central resource for neuronal morphologies. *J. Neurosci.* 27, 9247–9251. doi: 10.1523/JNEUROSCI.2055-07.2007
- Badel, L., Lefort, S., Brette, R., Petersen, C. C., Gerstner, W., and Richardson, M. J. (2008). Dynamic IV curves are reliable predictors of naturalistic pyramidal-neuron voltage traces. *J. Neurophysiol.* 99, 656–666. doi: 10.1152/jn.01107.2007
- Benda, J., and Herz, A. V. (2003). A universal model for spike-frequency adaptation. *Neural Comput.* 15, 2523–2564. doi: 10.1162/089976603322385063
- Beyeler, M., Carlson, K. D., Chou, T. S., Dutt, N., and Krichmar, J. L. (2015). “A user-friendly and highly optimized library for the creation of neurobiologically detailed spiking neural networks,” in *International Joint Conference on Neural Networks* (Killarney, IE).
- Brette, R., and Gerstner, W. (2005). Adaptive exponential integrate-and-fire model as an effective description of neuronal activity. *J. Neurophysiol.* 94, 3637–3642. doi: 10.1152/jn.00686.2005
- Buckmaster, P. S., Strowbridge, B. W., and Schwartzkroin, P. A. (1993). A comparison of rat hippocampal mossy cells and CA3c pyramidal cells. *J. Neurophysiol.* 70, 1281–1299. doi: 10.1152/jn.1993.70.4.1281
- Cardin, J. A., Carlén, M., Meletis, K., Knoblich, U., Zhang, F., Deisseroth, K., et al. (2009). Driving fast-spiking cells induces gamma rhythm and controls sensory responses. *Nature* 459, 663–667. doi: 10.1038/nature08002
- Carnevale, N. T., Tsai, K. Y., Claiborne, B. J., and Brown, T. H. (1997). Comparative electrotonic analysis of three classes of rat hippocampal neurons. *J. Neurophysiol.* 78, 703–720. doi: 10.1152/jn.1997.78.2.703
- Chevalyere, V., and Siegelbaum, S. A. (2010). Strong CA2 pyramidal neuron synapses define a powerful disinaptic cortico-hippocampal loop. *Neuron* 66, 560–572. doi: 10.1016/j.neuron.2010.04.013
- Chittajallu, R., Craig, M. T., McFarland, A., Yuan, X., Gerfen, S., Tricoire, L., et al. (2013). Dual origins of functionally distinct O-LM interneurons revealed by differential 5-HT3AR expression. *Nat. Neurosci.* 16, 1598–1607. doi: 10.1038/nn.3538

the George Mason University Libraries Open Access Publishing Fund.

ACKNOWLEDGMENTS

We thank Charise White, Diek Wheeler, Ernest Barreto, and Sumit Nanda for their contribution and valuable comments on improving this article.

SUPPLEMENTARY MATERIAL

The Supplementary Material for this article can be found online at: <https://www.frontiersin.org/articles/10.3389/fninf.2018.00008/full#supplementary-material>

- Chitwood, R. A., Hubbard, A., and Jaffe, D. B. (1999). Passive electrotonic properties of rat hippocampal CA3 interneurons. *J. Physiol.* 515, 743–756. doi: 10.1111/j.1469-7793.1999.743ab.x
- Deb, K. (2014). “Multi-objective optimization,” in *Search Methodologies*, eds E. Burke and G. Kendall (Boston, MA: Springer), 403–449.
- De Jong, K. A. (2006). *Evolutionary Computation: A Unified Approach*. Cambridge, MA: MIT Press.
- Desai, N. S. (2003). Homeostatic plasticity in the CNS: synaptic and intrinsic forms. *J. Physiol. Paris* 97, 391–402. doi: 10.1016/j.jphysparis.2004.01.005
- Desai, N. S., Rutherford, L. C., and Turrigiano, G. G. (1999). Plasticity in the intrinsic excitability of cortical pyramidal neurons. *Nat. Neurosci.* 2, 515–520. doi: 10.1038/9165
- Druckmann, S., Banitt, Y., Gidon, A., Schürmann, F., Markram, H., and Segev, I. (2007). A novel multiple objective optimization framework for constraining conductance-based neuron models by experimental data. *Front. Neurosci.* 1, 7–18. doi: 10.3389/neuro.01.1.1.001.2007
- Eliasmith, C., Stewart, T. C., Choo, X., Bekolay, T., DeWolf, T., Tang, Y., et al. (2012). A large-scale model of the functioning brain. *Science* 338, 1202–1205. doi: 10.1126/science.1225266
- Ermentrout, B., Pascal, M., and Gutkin, B. (2001). The effects of spike frequency adaptation and negative feedback on the synchronization of neural oscillators. *Neural Comput.* 13, 1285–1310. doi: 10.1162/08997660152002861
- Foster, W. R., and Ungar, L. H. (1993). Significance of conductances in Hodgkin-Huxley models. *J. Neurophysiol.* 70, 2502–2518. doi: 10.1152/jn.1993.70.6.2502
- Gerken, W., Purvis, L., and Butera, R. (2005). Genetic algorithm for optimization and specification of a neuron model. *Conf. Proc. IEEE Eng. Med. Biol. Soc.* 4, 4321–4323. doi: 10.1109/IEMBS.2005.1615421
- Golding, N. L., Mickus, T. J., Katz, Y., Kath, W. L., and Spruston, N. (2005). Factors mediating powerful voltage attenuation along CA1 pyramidal neuron dendrites. *J. Physiol.* 568(Pt 1), 69–82. doi: 10.1113/jphysiol.2005.086793
- Gulyás, A. I., Szabó, G. G., Ulbert, I., Holderith, N., Monyer, H., Erdélyi, F., et al. (2010). Parvalbumin-containing fast-spiking basket cells generate the field potential oscillations induced by cholinergic receptor activation in the hippocampus. *J. Neurosci.* 30, 15134–15145. doi: 10.1523/JNEUROSCI.4104-10.2010
- Hendrickson, P. J., Yu, G. J., Song, D., and Berger, T. W. (2016). A million-plus neuron model of the hippocampal dentate gyrus: critical role for topography in determining spatiotemporal network dynamics. *IEEE Trans. Biomed. Eng.* 63, 199–209. doi: 10.1109/TBME.2015.2445771
- Hodgkin, A. L., and Huxley, A. F. (1952). A quantitative description of membrane current and its application to conduction and excitation in nerve. *J. Physiol.* 117, 500–544. doi: 10.1113/jphysiol.1952.sp004764
- Izhikevich, E. M. (2001). Resonate-and-fire neurons. *Neural Networks* 14, 883–894. doi: 10.1016/S0893-6080(01)00078-8
- Izhikevich, E. M. (2003). Simple model of spiking neurons. *IEEE Trans. Neural Netw.* 14, 1569–1572. doi: 10.1109/TNN.2003.820440

- Izhikevich, E. M. (2007). *Dynamical Systems in Neuroscience*. Cambridge, MA: MIT Press.
- Izhikevich, E. M., and Edelman, G. M. (2008). Large-scale model of mammalian thalamocortical systems. *Proc. Natl. Acad. Sci. U.S.A.* 105, 3593–3598. doi: 10.1073/pnas.0712231105
- Jarsky, T., Roxin, A., Kath, W. L., and Spruston, N. (2005). Conditional dendritic spike propagation following distal synaptic activation of hippocampal CA1 pyramidal neurons. *Nat. Neurosci.* 8, 1667–1676. doi: 10.1038/nn1599
- Keren, N., Peled, N., and Korngreen, A. (2005). Constraining compartmental models using multiple voltage recordings and genetic algorithms. *J. Neurophysiol.* 94, 3730–3742. doi: 10.1152/jn.00408.2005
- Khare, V., Yao, X., and Deb, K. (2003). Performance scaling of multi-objective evolutionary algorithms,” in *Evolutionary Multi-Criterion Optimization*, eds C. M. Fonseca, P. J. Fleming, E. Zitzler, L. Thiele, and K. Deb (Berlin, Heidelberg: Lecture Notes in Computer Science; Springer), 2632.
- Luke, S., Panait, L., Balan, G., Paus, S., Skolicki, Z., Bassett, J., et al. (2015). *Ecj: A Java-Based Evolutionary Computation Research System*. Available online at: <https://cs.gmu.edu/~eclab/projects/ecj/>
- Lynch, E. P., and Houghton, C. J. (2015). Parameter estimation of neuron models using *in-vitro* and *in vivo* electrophysiological data. *Front. Neuroinform.* 9:10. doi: 10.3389/fninf.2015.00010
- Mainen, Z. F., Carnevale, N. T., Zador, A. M., Claiborne, B. J., and Brown, T. H. (1996). Electrotonic architecture of hippocampal CA1 pyramidal neurons based on three-dimensional reconstructions. *J. Neurophysiol.* 76, 1904–1923. doi: 10.1152/jn.1996.76.3.1904
- Marder, E., and Goaillard, J. M. (2006). Variability, compensation and homeostasis in neuron and network function. *Nat. Rev. Neurosci.* 7, 563–574. doi: 10.1038/nrn1949
- Marder, E., and Prinz, A. A. (2002). Modeling stability in neuron and network function: the role of activity in homeostasis. *Bioessays* 24, 1145–1154. doi: 10.1002/bies.10185
- Markram, H., Muller, E., Ramaswamy, S., Reimann, M. W., Abdellah, M., Sanchez, C. A., et al. (2015). Reconstruction and simulation of neocortical microcircuitry. *Cell* 163, 456–492. doi: 10.1016/j.cell.2015.09.029
- Oliva, A. A., Jiang, M., Lam, T., Smith, K. L., and Swann, J. W. (2000). Novel hippocampal interneuronal subtypes identified using transgenic mice that express green fluorescent protein in GABAergic interneurons. *J. Neurosci.* 20, 3354–3368.
- Padmanabhan, K., and Urban, N. N. (2010). Intrinsic biophysical diversity decorrelates neuronal firing while increasing information content. *Nat. Neurosci.* 13, 1276–1282. doi: 10.1038/nn.2630
- Pawelzik, H., Hughes, D. I., and Thomson, A. M. (2002). Physiological and morphological diversity of immunocytochemically defined parvalbumin- and cholecystokinin-positive interneurons in CA1 of the adult rat. *J. Comp. Neurol.* 443, 346–367. doi: 10.1002/cne.10118
- Pozzorini, C., Mensi, S., Hagens, O., and Naud, R. (2015). Automated high-throughput characterization of single neurons by means of simplified spiking models. *PLoS Comput. Biol.* 11:e1004275. doi: 10.1371/journal.pcbi.1004275
- Price, C. J., Cauli, B., Kovacs, E. R., and Kulik, A. (2005). Neurogliaform neurons form a novel inhibitory network in the hippocampal CA1 area. *J. Neurosci.* 25, 6775–6786. doi: 10.1523/JNEUROSCI.1135-05.2005
- Rossant, C., Goodman, D. F., Fontaine, B., Platkiewicz, J., Magnusson, A. K., and Brette, R. (2011). Fitting neuron models to spike trains. *Front. Neurosci.* 5:9. doi: 10.3389/fnins.2011.00009
- Rossant, C., Goodman, D., Platkiewicz, J., and Brette, R. (2010). Automatic fitting of spiking neuron models to electrophysiological recordings. *Front. Neuroinform.* 4:2. doi: 10.3389/neuro.11.002.2010
- Rössert, C., Pozzorini, C., Chindemi, G., Davison, A. P., Eroev, C., King, J., et al. (2016). Automated point-neuron simplification of data-driven microcircuit models. *arXiv:1604.00087v2*.
- Rounds, E. L., Scott, E. O., Alexander, A. S., De Jong, K. A., Nitz, D. A., and Krichmar, J. L. (2016). An evolutionary framework for replicating neurophysiological data with spiking neural networks,” in *International Conference on Parallel Problem Solving from Nature – PPSN XIV* (Edinburgh: Springer International Publishing), 537–547.
- Savić, N., and Sciancalepore, M. (2001). Electrophysiological characterization of “giant” cells in stratum radiatum of the CA3 hippocampal region. *J. Neurophysiol.* 85, 1998–2007. doi: 10.1152/jn.2001.85.5.1998
- Schulz, D. J., Goaillard, J. M., and Marder, E. (2006). Variable channel expression in identified single and electrically coupled neurons in different animals. *Nat. Neurosci.* 9, 356–362. doi: 10.1038/nn1639
- Traub, R. D., Whittington, M. A., Stanford, I. M., and Jefferys, J. G. (1996). A mechanism for generation of long-range synchronous fast oscillations in the cortex. *Nature* 383, 621–624. doi: 10.1038/383621a0
- Tripathy, S. J., Padmanabhan, K., Gerkin, R. C., and Urban, N. N. (2013). Intermediate intrinsic diversity enhances neural population coding. *Proc. Natl. Acad. Sci. U.S.A.* 110, 8248–8253. doi: 10.1073/pnas.1221214110
- Van Geit, W., De Schutter, E., and Achard, P. (2008). Automated neuron model optimization techniques: a review. *Biol. Cybern.* 99, 241–251. doi: 10.1007/s00422-008-0257-6
- Van Geit, W., Achard, P., and De Schutter, E. (2007). Neurofitter: a parameter tuning package for a wide range of electrophysiological neuron models. *Front. Neuroinform.* 1:1. doi: 10.3389/neuro.11.001.2007
- Wheeler, D. W., White, C. M., Rees, C. L., Komendantov, A. O., Hamilton, D. J., and Ascoli, G. A. (2015). Hippocampome.org: a knowledgebase of neuron types in the rodent hippocampus. *Elife* 4:e09960. doi: 10.7554/eLife.09960
- Wittner, L., and Miles, R. (2007). Factors defining a pacemaker region for synchrony in the hippocampus. *J. Physiol.* 584, 867–883. doi: 10.1113/jphysiol.2007.138131

Conflict of Interest Statement: The authors declare that the research was conducted in the absence of any commercial or financial relationships that could be construed as a potential conflict of interest.

Copyright © 2018 Venkadesh, Komendantov, Listopad, Scott, De Jong, Krichmar and Ascoli. This is an open-access article distributed under the terms of the Creative Commons Attribution License (CC BY). The use, distribution or reproduction in other forums is permitted, provided the original author(s) and the copyright owner are credited and that the original publication in this journal is cited, in accordance with accepted academic practice. No use, distribution or reproduction is permitted which does not comply with these terms.